

MASS OUTFLOW RATE FROM ACCRETION DISKS AROUND COMPACT OBJECTS

TAPAS K. DAS AND SANDIP K. CHAKRABARTI
S. N. Bose National Centre For Basic Sciences
Block JD Sector III Salt Lake Calcutta 700 091 India
Email: tdas@boson.bose.res.in, chakraba@boson.bose.res.in

Abstract.

We compute mass outflow rates from accretion disks around compact objects, such as neutron stars and black holes. These computations are done using combinations of exact transonic inflow and outflow solutions which may or may not form standing shock waves. Assuming that the bulk of the outflow is from the effective boundary layers of these objects, we find that the ratio of the outflow rate and inflow rate varies anywhere from a few percent to even close to a hundred percent (i.e., close to disk evacuation case) depending on the initial parameters of the disk, the degree of compression of matter near the centrifugal barrier, and the polytropic index of the flow. Our result, in general, matches with the outflow rates obtained through a fully time-dependent numerical simulation. In some region of the parameter space when the standing shock does not form, our results *indicate* that the disk may be evacuated and may produce quiescence states.

Published in *Classical and Quantum Gravity*; Vol. 16, No. 12. Pg. 3879

1. INTRODUCTION

One of the signatures of activities around compact objects is the presence of jets and outflows. Outflows carry away angular momentum from the accretion disk and are partially responsible for the accretion itself. Active galaxies and quasars are supposed to harbour black holes at their centers and at the same time produce cosmic radio jets through which immense

amount of matter and energy are ejected out of the core of the galaxies (See, [1-2] for a recent review). Similarly, micro-quasars have also been discovered very recently where outflows are formed from stellar black hole candidates [3]. Many of these outflows show superluminal motions which are probably due to magnetic effects. With hydrodynamic effects alone, which we are employing in this paper, one should not be able to accelerate the flow more than the initial sound velocity. A well known stellar object SS433 (which is believed to be a neutron star), where pure hydrodynamic effects may be operating, produces outflows with a speed roughly one-third of the speed of light.

There are several models in the literature which study the origin, formation and collimation of these outflows. Difference between stellar outflows and outflows from these systems is that the outflows in these systems have to form out of the inflowing material only. This is because black holes and neutron stars have no atmospheres of their own. The models present in the literature are roughly of three types. The first type of solutions confine themselves to the jet properties only, completely decoupled from the internal properties of accretion disks. They study the effects of hydrodynamic or magneto-hydrodynamic pressures on the origin of jets [4-6, Chap 3 of 1]. In the second type, efforts are made to correlate the internal disk structure with that of the outflow using both hydrodynamic [1] and magnetohydrodynamic considerations [7-8]. In the third type, numerical simulations are carried out to actually see how matter is deflected from the equatorial plane towards the axis [9-12]. From the analytical front, although the wind type solutions and accretion type solutions come out of the same set of governing equations [e.g. 7-8], there was no attempt to obtain the estimation of the outflow rate from the inflow rate. On the other hand, the mass outflow rate of the normal stars are calculated very accurately from the stellar luminosity. Theory of radiatively driven winds seems to be very well understood [13]. The simplicity of black holes and neutron stars lie in the fact that they do not have atmospheres. But the disks surrounding them have, and similar method as employed in stellar atmospheres should be applicable to the disks. Our approach in this paper is precisely this. We first determine the properties of the rotating inflow and outflow and identify solutions to connect them. In this manner we self-consistently determine the mass outflow rates.

Before we proceed, we describe basic properties of the rotating matter around a black hole. Rotating matter behaves in a special manner at two radial distances [14] — (a) marginally stable orbit (r_{ms}) and (b) marginally bound orbit (r_{mb}). For $r < r_{ms}$ no time-like orbit is stable. The corresponding Keplerian angular momentum is $\lambda_{ms} = 3.67GM/c$ for a Schwarzschild black hole of mass M , G and c being the universal gravitational constant

and velocity of light respectively. For $r < r_{mb}$, any closed orbit is impossible and matter must dive into a black hole. The corresponding Keplerian angular momentum is $\lambda_{mb} = 4GM/c$. Matter with a larger angular momentum ($\lambda > \lambda_{mb}$) must require a positive energy at infinity in order to enter into a black hole since the centrifugal barrier becomes otherwise unsurmountable (see, Fig. 12.3 of [14]). Thus, normally, for a black hole accretion, one is interested in flows with $\lambda < \lambda_{mb}$. The centrifugal force

$$F_c \sim \lambda^2/r^3 \quad (1a)$$

fighters against the gravitational force

$$F_g \sim -GM/r^2 \quad (1b)$$

and in a Keplerian disk (consists of a collection of closed timelike geodesics) these two forces balance. In exact form, the Keplerian distribution of specific angular momentum in Schwarzschild geometry is given by [14],

$$\lambda_{Kep} = \frac{\sqrt{GM}r}{1 - \frac{2GM}{c^2r}} \quad (2)$$

With this distribution, there is no centrifugal barrier left, since the two forces exactly cancel each other.

On the other hand, a rotating inflow with a specific angular momentum $\lambda(r)$ entering into a black hole will have angular momentum $\lambda \sim \text{constant}$ close to the black hole for any moderate viscous stress. Physically, this is due to fact that viscosity transports momentum, and therefore angular momentum to outer parts of the disk and it takes much longer time (than the infall time of matter) to do so. Problem with a constant angular momentum flow with $\lambda_{ms} < \lambda < \lambda_{mb}$ is that it must be sub-Keplerian [eq. (2)] for $r < r_{mb}$. A second, and more important reason why a flow must deviate from a Keplerian disk can be understood in the following way [15]: Consider a perfect fluid with the stress-energy tensor (using $G = c = M = 1$),

$$T_{\mu\nu} = \rho u_\mu u_\nu + p(g_{\mu\nu} + u_\mu u_\nu) \quad (3)$$

where, p is the pressure and $\rho = \rho_0(1 + \pi)$ is the mass density, π being the internal energy. We assume the vacuum metric around a Kerr black hole to be of the form [14]

$$ds^2 = g_{\mu\nu} dx^\mu dx^\nu = -\frac{r^2 \Delta}{A} dt^2 + \frac{A}{r^2} (d\phi - \omega dt)^2 + \frac{r^2}{\Delta} dr^2 + dz^2 \quad (4)$$

Where,

$$A = r^4 + r^2 a^2 + 2ra^2; \quad \Delta = r^2 - 2r + a^2; \quad \omega = \frac{2ar}{A}$$

Here, $g_{\mu\nu}$ is the metric coefficient and u^μ is the four velocity component.

$$u_t = \left[\frac{\Delta}{(1 - V^2)(1 - \Omega\lambda)(g_{\phi\phi} + \lambda g_{t\phi})} \right]^{1/2}. \quad (5)$$

Here, $\lambda = -u_\phi/u_t$ is the specific angular momentum and $\Omega = u^\phi/u^t$. On the horizon, for *all* a , $\Delta = 0$. Since all the other terms behave smoothly, V must be unity, i.e., velocity of light. Since in the extreme equation of state of $p = \rho/3$, the sound speed is $1/\sqrt{3}$. Thus the Mach number is larger than unity, and the flow must be supersonic on the horizon. A supersonic flow is always sub-Keplerian [1]. It is to be noted that the investigations made so far are from Keplerian disks only. In the present paper, we investigate outflow formation from more realistic flows which are necessarily sub-Keplerian.

Going back to equations (1a) and (1b), one notes that the F_c increases much faster compared to the F_g and becomes comparable at around $r_{cb} \sim \lambda^2/GM$. (In the rest of the paper, we use $R_g = 2GM/c^2$ as the length unit, c is the unit of velocity, and the mass of the black hole M to the unit of mass.) Here, (actually, a little farther out, due to thermal pressure) matter starts piling up and produces the centrifugal pressure supported boundary layer (CENBOL for short). Further close to the black hole, the gravity always wins and matter enters the horizon supersonically after passing through a sonic point. This centrifugal pressure supported region, may or may not have a sharp boundary, depending on whether standing shocks form or not (see [1] for references). Generally speaking, in a polytropic flow, if the polytropic index $\gamma > 1.5$, then shocks do not form and if $\gamma < 1.5$, only a region of the parameter space forms the shock [1]. In this layer (CENBOL) the flow becomes hotter and denser and for all practical purposes behaves as the stellar atmosphere so far as the formation of outflows are concerned. Inflows on neutron stars behave similarly, except that the ‘hard-surface’ inner boundary condition dictates that the flow remains subsonic between the CENBOL and the surface rather than becoming supersonic as in the case of a black hole. In case where the shock does not form, regions around pressure maximum achieved just outside the inner sonic point would also drive the flow outwards. In the back of our mind, we have the picture of the outflow as obtained by numerical simulations [11], namely, that the outflow is thermally and centrifugally accelerated but confined by external pressure of the ambient medium.

At a first glance, it may be astonishing that a black hole, which has no hard surface, should allow a ‘boundary layer’ or CENBOL. Observationally, in the context of spectral properties of black hole candidates, the presence of this boundary layer has been established long ago (see, [1-2, 16]). It turns out that most of hard X-rays from black hole accretion disk comes out of

Outflow rates from accretion disks around black hole and neutron stars must be related to the properties of CENBOL which in turn, depend on the inflow parameters. Subsonic outflows originating from CENBOL would pass through sonic points and reach far distances as in wind solutions. Assuming free-falling conical polytropic inflow and isothermal outflows (as in stellar winds), it is easy to estimate the ratio of outflowing and inflowing rates [2, 22]:

$$\frac{\dot{M}_{out}}{\dot{M}_{in}} = R_{in} = \frac{\Theta_{out}}{\Theta_{in}} \frac{R}{4} e^{-(f_0 - \frac{3}{2})} f_0^{3/2} \quad (6)$$

where, Θ_{out} and Θ_{in} are the solid angles of the outflow and inflow respectively, and

$$f_0 = \frac{(2n + 1)R}{2n}. \quad (7)$$

Here, R is the compression ratio of inflowing matter at the CENBOL and $n = 1/(\gamma - 1)$ is the polytropic constant. When $\Theta_{out} \sim \Theta_{in}$, $R_{in} \sim 0.052$ and 0.266 for $\gamma = 4/3$ and $5/3$ respectively. Assuming a thin inflow and outflow of 10° conical angle, the ratio R_{in} becomes 0.0045 and 0.023 respectively.

The aim of the present paper is to compute the mass loss rate more realistically than what has been attempted so far. We calculate this rate as a function of the inflow parameters, such as specific energy and angular momentum, accretion rate, polytropic index etc. We explore both the polytropic and the isothermal outflows. Our conclusions show that the outflow rate is sensitive to the specific energy and accretion rate of the inflow. Specifically, when the outflow is not isothermal, outflow rate generally increases with the specific energy and the polytropic index γ_o of the outflow, generally decreases with the polytropic index γ of the inflow, but somewhat insensitive to the specific angular momentum λ . In the case of isothermal outflow, however, mass loss rate is sensitive to the inflow rate, since the inflow rate decides the proton temperature of the advective region of the disk which in turn fixes the outflow temperature. In this case the outflow is at least partially temperature driven. The outflow rate is also found to be anti-correlated with specific angular momentum λ of the flow.

The plan of this paper is the following: In the next Section, we describe our model and present the governing equations for the inflow and outflow. In §3, we present the solution procedure of the equations. In §4, we present results of our computations. Finally, in §5, we draw our conclusions. A preliminary report of this kind has been published elsewhere [23].

2. Model Description and Governing Equations

2.1. INFLOW MODEL

For the sake of computation of the inflow quantities, we assume that the inflow is axisymmetric and thin: $h(r) \ll r$, so that the transverse velocity component could be ignored compared to the radial and azimuthal velocity components. We consider polytropic inflows in vertical equilibrium (otherwise known as 1.5 dimensional flows [21]). We ignore the self-gravity of the flow. We do the calculations using Paczyński-Wiita [24] potential which mimics surroundings of the Schwarzschild black hole. The equations (in dimensionless units) governing the inflow are:

(a) Conservation of specific energy is given by,

$$\mathcal{E} = \frac{u_e^2}{2} + na_e^2 + \frac{\lambda^2}{2r^2} - \frac{1}{2(r-1)}. \quad (8)$$

where, u_e and a_e are the radial and polytropic sound velocities respectively. $a_e = (\gamma p_e / \rho_e)^{1/2}$, p_e and ρ_e are the pressure and density of the flow. For a polytropic flow, $p_e = K \rho_e^\gamma$, where K is a constant and is a measure of entropy of the flow. Here, λ is the specific angular momentum and n is the polytropic constant of the inflow $n = (\gamma - 1)^{-1}$, γ is the polytropic index. The subscript e refers that the quantities are measured on the equatorial plane.

Mass conservation equation, apart from a geometric constant, is given by,

$$\dot{M}_{in} = u_e \rho_e r h_e(r), \quad (9)$$

where $h_e(r)$ is the half-thickness of the flow at radial co-ordinate r having the following expression

$$h_e(r) = a_e r^{\frac{1}{2}} (r-1) \sqrt{\frac{2}{\gamma}}. \quad (10a)$$

Another useful way of writing the mass inflow is to introduce an entropy dependent quantity $\dot{\mathcal{M}} \propto \gamma^n K^n \dot{M}$ which can be expressed as

$$\dot{\mathcal{M}} = u_e a_e^\alpha r^{\frac{3}{2}} (r-1) \sqrt{\frac{2}{\gamma}} \quad (10b)$$

Where, $\dot{\mathcal{M}}$ is really the entropy accretion rate [21]. When the shock is not present, $\dot{\mathcal{M}}$ remains constant in a polytropic flow. When the shock is present, $\dot{\mathcal{M}}$ will increase at the shock due to increase of entropy. $\alpha =$

$(\gamma + 1)/(\gamma - 1) = 2n + 1$. If the centrifugal pressure supported shock is present, the usual Rankine-Hugoniot conditions, namely, conservations of mass, energy and momentum fluxes across the shock are to be taken into account [21] in determining the shock locations. In presence of mass loss one must incorporate this effect in the shock condition (see, eq. 22 below).

2.2. OUTFLOW MODELS

We consider two types of outflows. In ordinary stellar mass loss computations [25], the outflow is assumed to be isothermal till the sonic point. This assumption is probably justified, since copious photons from the stellar atmosphere deposit momenta on the slowly outgoing and expanding outflow and possibly make the flow close to isothermal. This need not be the case for outflows from compact sources. Centrifugal pressure supported boundary layers close to the black hole are very hot (close to the virial temperature) and most of the photons emitted may be swallowed by the black holes themselves instead of coming out of the region and depositing momentum onto the outflow. Thus, the outflows could be cooler than isothermal flows. In our first model, we choose polytropic outflows with same energy as the inflow (i.e., no energy dissipation between the inflow and outflow) but with a different polytropic index $\gamma_o < \gamma$. Nevertheless, it may be advisable to study the isothermal outflow to find out the behavior of the extreme case. Thus an isothermal outflow is chosen in our second model. In each case, of course, we include the possibility that the *inflow* may or may not have standing shocks.

On the one hand, our assumption of thin inflow is for the sake of computation of the thermodynamic quantities only, but the flow itself need not be physically thin. Secondly, the funnel wall and the centrifugal barrier are purely geometric surfaces, and they exist anyway and the outflow could be supported even by ambient medium which may not necessarily be a part of the disk itself. So, we believe that our assumptions are not unjustified.

2.2.1. Polytropic Outflow

In this case, the energy conservation equation takes the form:

$$\mathcal{E} = \frac{v^2}{2} + n' a_e^2 + \frac{\lambda^2}{2r_m^2(r)} - \frac{1}{2(r-1)} \quad (11)$$

and the mass conservation in the outflow takes the form:

$$\dot{M}_{out} = \rho v \mathcal{A}(r). \quad (12)$$

Here, $n' = (\gamma_o - 1)^{-1}$ is the polytropic constant of the outflow. The difference between eq. (4) and eq. (1) is that, presently, the rotational energy

term contains

$$r_m(r) = \frac{\mathfrak{R}(r) + R(r)}{2}, \quad (13a)$$

as the mean *axial* distance of the flow. The expression of $\mathfrak{R}(r)$, the local radius of the centrifugal barrier comes from balancing the centrifugal force with the gravity [11], i.e.,

$$\frac{\lambda^2}{\mathfrak{R}^3(r)} = \frac{\mathfrak{R}(r)}{2r(r-1)^2}. \quad (13b)$$

We thus obtain,

$$\mathfrak{R}(r) = \left[2\lambda^2 r(r-1)^2\right]^{\frac{1}{4}} \quad (14a)$$

And the expression for $R(r)$, the local radius of the funnel wall, comes from vanishing of total effective potential, i.e.,

$$\Omega_{tot\,eff}(r) = -\frac{1}{2(r-1)} + \frac{\lambda^2}{2R^2(r)} = 0$$

$$R(r) = \lambda [(r-1)]^{1/2} \quad (14b)$$

The difference between eq. (12) and eq. (9) is that the area functions are different. Here, $A(r)$ is the area between the centrifugal barrier and the funnel wall (see introduction for the motivation). This is computed with the assumption that the outflow is external pressure supported, i.e., the centrifugal barrier is in pressure balanced with the ambient medium. Matter, if pushed hard enough, can cross centrifugal barrier in black hole accretion (the reason why rapidly rotating matter can enter into a black hole in the first place). An outward thermal force (such as provided by the CENBOL) in between the funnel wall and the centrifugal barrier causes the flow to come out. Thus the cross section of the outflow is,

$$\mathcal{A}(r) = \pi[\mathfrak{R}^2(r) - R^2(r)]. \quad (15)$$

The outflow angular momentum λ is chosen to be the same as in the inflow, i.e., no viscous dissipation is assumed to be present in the inner region of the flow close to a black hole. Considering that viscous time scales are longer compared to the inflow time scale, it may be a good assumption in the disk, but it may not be a very good assumption for the outflows which are slow prior to the acceleration and are therefore, prone to viscous transport of angular momentum. Such detailed study has not been attempted here particularly because we know very little about the viscous processes taking place in the pre-jet flow. Therefore, we concentrate only those cases where the specific angular momentum is roughly constant when inflowing matter

becomes part of the outflow, although some estimates of the change in R_{in} is provided when the average angular momentum of the outflow is lower. Detailed study of the outflow rates in presence of viscosity and magnetic field is in progress and would be presented elsewhere.

2.2.2. Isothermal Outflow

The integration of the radial momentum equation yields an equation similar to the energy equation (eq. 11):

$$\frac{\vartheta_{iso}^2}{2} + C_s^2 \ln \rho + \frac{\lambda^2}{2r_m(r)^2} - \frac{1}{2(r-1)} = \text{Constant} \quad (16)$$

In this case the thermal energy term is different, behaving logarithmically. The constant sound speed of the outflow is C_s . The mass conservation equation remains the same:

$$\dot{M}_{out} = \rho \vartheta_{iso} \mathcal{A}(r). \quad (17)$$

Here, the area function remains the same above. A subscript *iso* of velocity ϑ is kept to distinguish from the velocity in polytropic case. This is to indicate the velocities are measured here using completely different assumptions.

In both the models of the outflow, we assume that the flow is primarily radial. Thus the θ -component of the velocity is ignored ($\vartheta_\theta \ll \vartheta$).

3. Procedure to solve for disks and outflows simultaneously

Before we go into the details, a general understanding of the transonic flows around a black hole is essential. In [1, 21], all the solution topologies of the polytropic flow in pseudo-Newtonian geometry has been provided. In regions **I** and **O** of the parameter space the flow has only one sonic point. Matter with positive energy at a large distance must pass through that point before entering into the black hole supersonically. In regions **SA** and **SW** shocks may form in accretion and winds respectively, but no shocks are expected in winds and accretions if parameters are chosen from these branches. In **NSW** and **NSA**, two saddle type sonic points exist, but no steady shock solutions are possible.

Suppose that matter first enters through the outer sonic point and passes through a shock. At the shock, part of the incoming matter, having higher entropy density is likely to return back as winds through a sonic point, other than the one it just entered. Thus a combination of topologies, one from the region **SA** and the other from the region **O** is required to obtain a full solution. In the absence of the shocks, the flow is likely to bounce back at the pressure maximum of the inflow and since the outflow

would be heated by photons, and thus have a smaller polytropic constant, the flow would leave the system through an outer sonic point different from that of the incoming solution. Thus finding a complete self-consistent solution boils down to finding the outer sonic point of the outflow and the mass flux through it. Below we present the list of parameters used in both of our models and briefly describe the procedure to obtain a satisfactory solution.

3.1. POLYTROPIC OUTFLOW

We assume that

(a) In this case, a very little amount of total energy is assumed to be lost in each bundle of matter as it leaves the disk and joins the jet. The specific energy \mathcal{E} remains fixed throughout the flow trajectory as it moves from the disk to the jet.

(b) Very little viscosity is present in the flow except at the place where the shock forms, so that the specific angular momentum λ is constant in both inflows and outflows close to the black hole. At the shock, entropy is generated and hence the outflow is of higher entropy for the same specific energy.

(c) The polytropic index of the inflow (γ) and outflow (γ_o) are free parameters and in general, $\gamma_o < \gamma$, because of heating effect of the outflow (e.g., due to the momentum deposition coming out of the disk surface). In reality γ_o is directly related to the heating and cooling processes of the outflow. When \dot{M}_{in} is high, heating of outflow by photon momentum deposition is higher, and therefore $\gamma_o \rightarrow 1$.

Thus a supply of parameters \mathcal{E} , λ , γ and γ_o make a self-consistent computation of R_{in} possible when the shock is present. When the shock is absent, the compression ratio of the gas at the pressure maximum between the inflow and outflow R_{comp} is supplied as a free parameter, since it may be otherwise very difficult to compute satisfactorily. In the presence of shocks, such problems do not arise as the compression ratio is obtained self-consistently.

The following procedure is adopted to obtain a complete solution:

(a) From eqs. (8) and (9) we derive an expression for the derivative,

$$\frac{du}{dr} = \left(\frac{\frac{\lambda^2}{r^3} + \frac{na^2}{\alpha} + \frac{5r-3}{r(r-1)} - \frac{1}{2(r-1)^2}}{u - \frac{2na^2}{\alpha u}} \right). \quad (18)$$

At the sonic point, the numerator and denominator separately vanish, and give rise to the so-called sonic point conditions:

$$a_c = \left(\frac{\frac{1}{2(r_c - 1)^2} - \frac{\lambda^2}{r_c^3}}{\frac{\alpha(r_c - 1)r_c}{n(5r_c - 3)}} \right) \quad (19a)$$

$$u_c = \sqrt{\frac{2n}{\alpha}} a_c \quad (19b)$$

where, the subscript c represents the quantities at the sonic point. The derivative of the flow at the sonic point is computed using the L'Hospital's rule. Using fourth order Runge-Kutta method $\vartheta(r)$ and $a(r)$ are computed along the flow till the position where the Rankine-Hugoniot condition is satisfied (if shocks form) and from there on the sub-sonic branch is integrated for the accretion as usual. With the known γ_o , \mathcal{E} and λ , one can compute the location of the outflow sonic point from eqs. (11) and (12),

$$\frac{d\vartheta}{dr} = \left(\frac{\frac{a^2}{\mathcal{A}^2(r)} \frac{d\mathcal{A}(r)}{dr} + \frac{\lambda^2}{r_m^3(r)} \frac{dr_m(r)}{dr} - \frac{1}{2(r-1)^2}}{\vartheta - \frac{a^2}{\vartheta}} \right) \quad (20)$$

from where the sonic point conditions at the outflow sonic point r_{co} obtained are given by,

$$\frac{a_{co}^2}{\mathcal{A}_{co}^2(r)} \frac{d\mathcal{A}(r)}{dr} \Big|_{co} + \frac{\lambda^2}{r_{mco}^3(r)} \frac{dr_m(r)}{dr} \Big|_{co} - \frac{1}{2(r_{co} - 1)^2} = 0 \quad (21a)$$

and

$$\vartheta_{co} = a_{co}. \quad (21b)$$

At the outer sonic point, the derivative of ϑ is computed using the L'Hospital's rule and the Runge-Kutta method is used to integrate towards the black hole to compute the velocity of the outflow at the shock location. The density of the outflow at the shock is computed by distributing the post-shock dense matter of the disk into spherical shell of 4π solid angle. The outflow rate is then computed using eq. (12).

It is to be noted that when the outflows are produced, one cannot use the usual Rankine-Hugoniot relations at the shock location, since mass flux is no longer conserved *in accretion*, but part of it is lost in the outflow. Accordingly, we use,

$$\dot{M}_+ = (1 - R_{\dot{m}}) \dot{M}_- \quad (22)$$

where, the subscripts + and – denote the pre- and post-shock values respectively. Since due to the loss of matter in the post-shock region, the post-shock pressure goes down, the shock recedes backward for the same value of incoming energy, angular momentum & polytropic index. The combination of three changes, namely, the increase in the cross-sectional area of the outflow and the launching velocity of the outflow and the decrease in the post-shock density decides whether the net outflow rate would increased or decreased than from the case when the exact Rankine-Hugoniot relation was used.

In the case where the shocks do not form, the procedure is a bit different. It is assumed that the maximum amount of matter comes out from the place of the disk where the thermal pressure of the inflow attains its maximum. The expression for the polytropic pressure for the inflow in vertical equilibrium is,

$$\mathcal{P}_e(r) = \frac{a_e^{2(n+1)} \dot{M}_{in}}{\gamma^{(1+n)} \mathcal{M}} \quad (23)$$

This is maximized and the outflow is assumed to have the same quasi-conical shape with annular cross-section $\mathcal{A}(r)$ between the funnel wall and the centrifugal barrier as already defined. In the absence of shocks the compression ratio of the flow between the incoming flow and outgoing flow at the pressure maximum cannot be computed self-consistently unlike the case when the shock was present. Thus this ratio is chosen freely. We take the guidance for this number from what was obtained in the case when shocks are formed. However, in this case even when the mass loss takes place, *the location* of the pressure maximum remains unchanged. Since the compression ratio R_{comp} is a free parameter, R_{in} remains unchanged for a given R_{comp} . Let us assume that $\dot{\mu}_-$ is the *actual* mass inflow rate and it is same before and after the pressure maximum had the mass loss rate been negligible. Let $\dot{\mu}_+$ be the mass inflow rate *after* the pressure maximum, when the loss due to outflow is taken into account. Then, by definition, $\dot{\mu}_- = \dot{M}_{out} + \dot{\mu}_+$ and $R_{in} = \dot{M}_{out}/\dot{\mu}_-$. Thus the *actual* ratio of the mass outflow rate and the mass inflow rate, when the mass loss is taken into consideration is given by,

$$\frac{\dot{M}_{out}}{\dot{\mu}_+} = \frac{R_{in}}{1 - R_{in}}. \quad (24a)$$

However, this static consideration is valid only when $R_{in} < 1$. Otherwise, we must have,

$$-\frac{dM_{disk}}{dt} + \dot{\mu}_- = \dot{\mu}_+ + \dot{M}_{out}$$

i.e.,

$$-\frac{dM_{disk}}{dt} = \dot{\mu}_-(R_{in} - 1) + \dot{\mu}_+ \quad (24b)$$

Here, M_{disk} is the instantaneous mass of the disk. Since $R_{in} > 1$, the disk has to evacuate. These cases hint that the assumptions of the steady solution break down completely and the solutions may become highly time dependent.

3.2. ISOTHERMAL OUTFLOW

We assume that

(a) The outflow has exactly the *same* temperature as that of the post-shock flow, but the energy is not conserved as matter goes from disk to the jet. In other words the outflow is kept in a thermal bath of temperature as that of the post-shock flow.

(b) Same as (b) of §3.1.

(c) The post-shock proton temperature is determined from the inflow accretion rate \dot{M}_{in} using the consideration of Comptonization of the advective region. The procedure to compute typical proton temperature as a function of the incoming accretion rate has been adopted from [26].

(d) The polytropic index of the inflow can be varied but that of the outflow is always unity.

Thus a supply of parameters \mathcal{E} , λ and γ makes a self-consistent computation of R_{in} possible when the shock is present. When the shock is absent, the compression ratio of the gas at the pressure maximum between the inflow and the outflow R_{comp} is supplied as a free parameter exactly as in the polytropic case.

The following procedure is adopted to obtain a complete solution:

(a) From eqs. (16) and (17) we derive an expression for the derivative,

$$\frac{d\vartheta}{dr}|_{iso} = \left(\frac{\frac{C_s^2}{\mathcal{A}(r)} \frac{d\mathcal{A}(r)}{dr} + \frac{\lambda^2}{r_m^3(r)} \frac{dr_m(r)}{dr} - \frac{1}{2(r_c - 1)^2}}{\vartheta_{iso} - \frac{C_s^2}{\vartheta_{iso}}} \right). \quad (25)$$

At the sonic point, the numerator and denominator separately vanish, and give rise to the so-called sonic point conditions:

$$\frac{C_s^2}{\mathcal{A}_{co}(r)} \frac{d\mathcal{A}(r)}{dr}|_{co} + \frac{\lambda^2}{r_{mco}^3(r)} \frac{dr_m(r)}{dr}|_{co} - \frac{1}{2(r_{co} - 1)^2} = 0, \quad (26a)$$

and

$$\vartheta_{co} = C_s, \quad (26b)$$

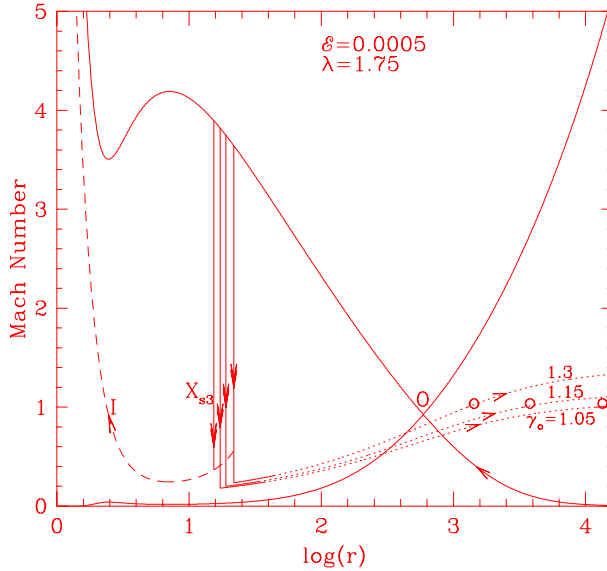


Fig. 2: Few typical solutions which combine accretion and outflow. Input parameters are $\mathcal{E} = 0.0005$, $\lambda = 1.75$ and $\gamma = 4/3$. Solid curve with an incoming arrow represents the pre-shock region of the inflow and the dashed curve with an incoming arrow represents post-shock inflow which enters the black hole after passing through the inner sonic point (I). Dotted curves are the outflows for various γ_o (marked). Open circles are sonic points of the outflowing winds and the crossing point ‘O’ is the outer sonic point of the inflow. The leftmost shock transition (X_{s3}) is obtained from unmodified Rankine-Hugoniot condition, while the other transitions are obtained when the mass-outflow is taken into account.

where, the subscript co represents the quantities at the sonic point of the outflow. The derivative of the flow at the sonic point is computed using the L’Hospital’s rule. The procedure is otherwise similar to those mentioned in the polytropic case and we do not repeat them here.

4. Results

4.1. POLYTROPIC OUTFLOW COMING FROM THE POST-SHOCK ACCRETION DISK

Figure 2 shows a typical solution which combines the accretion and the outflow. The input parameters are $\mathcal{E} = 0.0005$, $\lambda = 1.75$ and $\gamma = 4/3$ corresponding to relativistic inflow. The solid curve with an arrow represents the pre-shock region of the inflow and the long-dashed curve representn

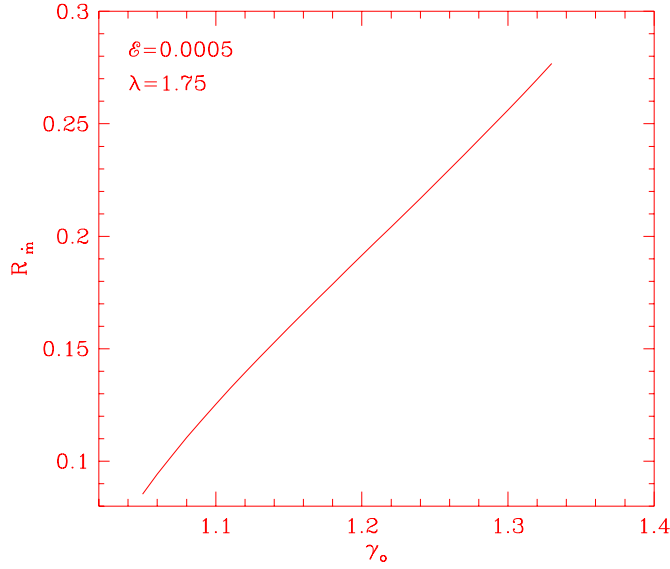


Fig. 3: Ratio $R_{\dot{m}}$ as outflowing polytropic index γ_o is varied. Only the range of γ_o for which the shock-solution is present is shown here. As γ_o is increased, the ratio is also increased. Since γ_o is generally anti-correlated with \dot{m}_{in} , this implies that $R_{\dot{m}}$ is correlated with \dot{m}_{in} .

the post-shock inflow which enters the black hole after passing through the inner sonic point (I). The solid vertical line at X_{s3} (the leftmost vertical transition) with double arrow represents the shock transition obtained with exact Rankine-Hugoniot condition (i.e., with no mass loss). The actual shock location obtained with modified Rankine-Hugoniot condition (eq. 22) is farther out from the original location X_{s3} . Three vertical lines connected with the corresponding dotted curves represent three outflow solutions for the parameters $\gamma_o = 1.3$ (top), 1.15 (middle) and 1.05 (bottom). The outflow branches shown pass through the corresponding sonic points. It is evident from the figure that the outflow moves along solution curves completely different from that of the ‘wind solution’ of the inflow which passes through the outer sonic point ‘O’. The mass loss ratio $R_{\dot{m}}$ in these cases are 0.256, 0.159 and 0.085 respectively. Figure 3 shows the ratio $R_{\dot{m}}$ as γ_o is varied. Only the range of γ_o and energy for which the shock-solution is present is shown here. The general conclusion is that as γ_o is increased the ratio is also increased non-linearly. When the inflow rate is very low, due to paucity of the photons, the outflow is not heated very much and γ_o remains higher. The reverse is true when the accretion rate is higher.

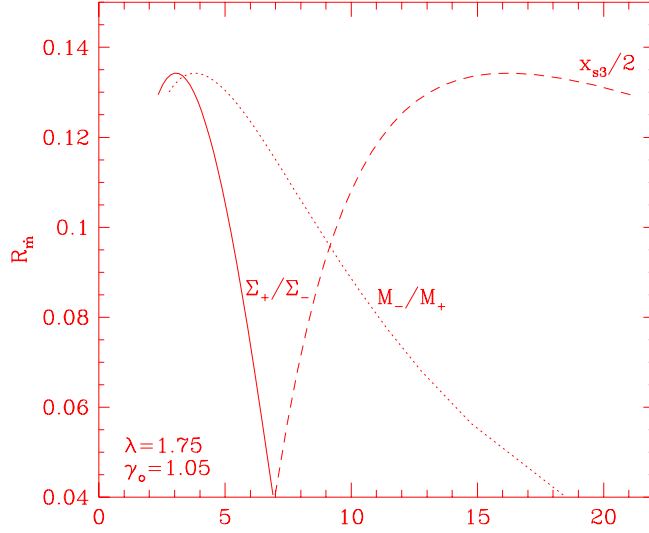


Fig. 4a: Variation of $R_{\dot{m}}$ as a function of (a) shock-strength M_-/M_+ (dotted) compression ratio Σ_+/Σ_- (solid) and the shock location X_{s3} (dashed) for $\gamma_o = 1.05$.

Thus, effectively, the ratio $R_{\dot{m}}$ is going up with the decrease in \dot{M}_{in} . In passing we remark that with the variation in the inflow angular momentum, λ , the result does not change significantly, and $R_{\dot{m}}$ changes only by a couple of percentage at the most.

In Fig. 4a, we show the variation of the ratio $R_{\dot{m}}$ of the mass outflow rate and inflow rate as a function of the shock-strength (dotted) M_-/M_+ (Here, M_- and M_+ are the Mach numbers of the pre- and post-shock flows respectively.), the compression ratio (solid) Σ_+/Σ_- (Here, Σ_- and Σ_+ are the vertically integrated matter densities in the pre- and post- shock flows respectively), and the stable shock location (dashed) X_{s3} (in the notation of [21]). Other parameters are $\lambda = 1.75$ and $\gamma_o = 1.05$. Note that the ratio $R_{\dot{m}}$ does not peak near the strongest shocks! Shocks are stronger when they are located closer to the black hole, i.e., for smaller energies. The non-monotonic behavior is more clearly seen in lowest curve of Fig. 4b where $R_{\dot{m}}$ is plotted as a function of the specific energy \mathcal{E} (along x-axis) and γ_o (marked on each curve). Specific angular momentum is chosen to be $\lambda = 1.75$ as before. The tendency of the peak in $R_{\dot{m}}$ is primarily because as \mathcal{E} is increased, the shock location is increased which generally increases the outflowing area $\mathcal{A}(r)$ at the shock location. However, the density of the

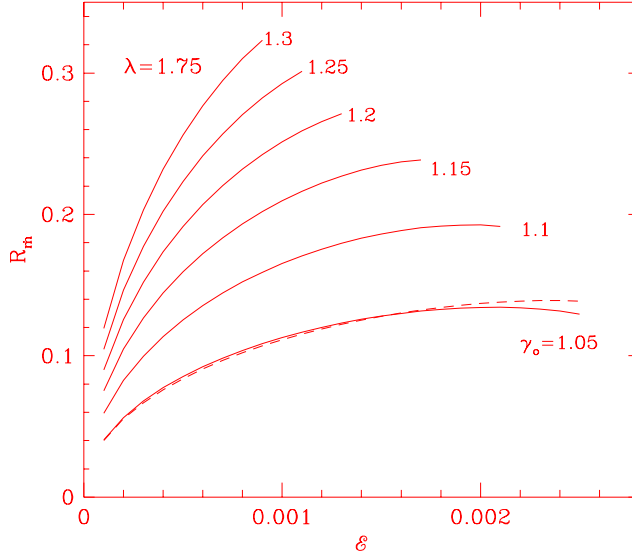


Fig. 4b: Variation of $R_{\dot{m}}$ as a function of specific energy \mathcal{E} for various γ_o (marked). $\lambda = 1.75$ throughout. .

outflow at the shock,

as well as the velocity of the outflow at the shock increases. The outflow rate, which is a product of these quantities, thus shows a peak. For the sake of comparison, we present the results for $\gamma_o = 1.05$ (dashed curve) when the Rankine-Hugoniot relation was not corrected by eq. (22). The result generally remains the same because of two competing effects: decrease in post-shock density and increase in the area from the the outflow is launched (i.e., area between the black hole and the shock) as well as the launching velocity of the jet at the shock.

To have a better insight of the behavior of the outflow we plot in Fig. 5 $R_{\dot{m}}$ as a function of the polytropic index of the *incoming* flow (γ) for $\gamma_o = 1.1$, $\mathcal{E} = 0.002$ and $\lambda = 1.75$. The range of γ shown is the range for which shock forms in the flow. We also plot the variation of injection velocity ϑ_{inj} , injection density ρ_{inj} and area $\mathcal{A}(r)$ of the outflow at the location where the outflow leaves the disk. The incoming accretion rate has been chosen to be 0.3 (in units of the Eddington rate). These quantities are scaled from the corresponding dimensionless quantities as $\vartheta_{inj} \rightarrow 0.1\vartheta_{inj}$, $\rho_{inj} \rightarrow 10^{22}\rho_{inj}$ and $\mathcal{A} \rightarrow 10^{-4}\mathcal{A}$ respectively in order to bring them in the same scale. With the increase in γ , the shock location is increased, and therefore the cross-sectional area of the outflow goes up.

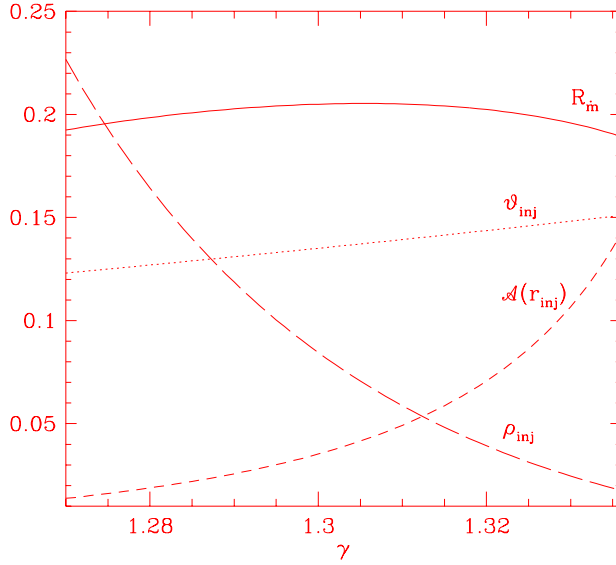


Fig. 5: $R_{\dot{m}}$ as a function of the polytropic index γ of the inflow. The range of γ shown is the range for which shock forms in the flow. Suitably scaled density, velocity and area of the flow (at the base of the outflow) on the disk surface are also shown. See text for details. Non-monotonicity in $R_{\dot{m}}$ can be understood by the fact that the shock location, i.e., the area $\mathcal{A}(r_{inj})$ and velocity v_{inj} of the outflow *at the outflow origin* go up with γ , but the density ρ_{inj} goes down.

The injection velocity goes up (albeit very slowly) as the shock recedes, since the injection surface (CENBOL) comes closer to the outflow sonic point. However, the density goes down (gas is less denser). This anti-correlation is reflected in the peak of $R_{\dot{m}}$.

So far, we assumed that the specific angular momentum of the outflow is exactly the same as that of the inflow, while in reality it could be different due to presence of viscosity. In the outflow, a major source of viscosity is the radiative viscosity whose coefficient is,

$$\eta = \frac{4aT^4}{15\kappa_T c\rho} \text{ cm}^2 \text{ sec}^{-1} \quad (27)$$

This could be significant, since the temperature of the outflow is high, but the density is low. Assuming that the angular momentum distribution reaches a steady state inside the jet ([1] and references therein),

$$l_j = C_j R^{n_j} \quad (28)$$

where C_j and n_j are constants, the vanishing condition of the azimuthal velocity on the axis requires that $n_j > 1$ inside the jet. The matter distribution in the *rotationally dominant* region of the ‘pre-jet’ is computed by integrating Euler equation. It is easy to show that the ‘hollow’ jet thus produced carry most of the matter and angular momentum in the outer layers of the jet [1]. In other words, the average angular momentum of the outflow *away from the base* may remain roughly constant even in presence of viscosity. This is to be contrasted with the disk, where matter is more dense towards the centre while more angular momentum is concentrated towards the outer edge. If, however, the average angular momentum *at the base* of the outflow goes down due to losses to ambient medium, by, say, a factor of two, we find that the mass loss rate is also reduced by around the same factor. This shows that the outflow is at least partially centrifugally driven.

An important point to note: the ratio between the ‘specific entropy measure’ of the outflow to that of the post-shock inflow is obtained from the definitions of entropy accretion rate $\dot{\mathcal{M}}$:

$$\frac{K_o}{K_+} = \frac{\dot{\mathcal{M}}_{out}^{\gamma_o-1}}{\dot{\mathcal{M}}_+^{\gamma-1}} \left(\frac{1 - R_{in}}{R_{in}} \right)^{\gamma_o-1} \dot{M}_+^{(\gamma-\gamma_o)} \frac{\gamma}{\gamma_o} \quad (29)$$

As $R_{in} \rightarrow 1$, $\frac{K_o}{K_+} \rightarrow 0$. Thus, we expect that for a polytropic flow with shocks, a hundred percent outflow is impossible since the outgoing entropy must be higher. In isothermal outflows such simple consideration do not apply.

If we introduce an extra radiation pressure term (with a term like Γ/r^2 in the radial force equation, where Γ is the contribution due to radiative process), particularly important for neutron stars, the outcome is significant. In the inflow, outward radiation pressure weakens gravity and thus the shock is located farther out. The temperature is cooler and therefore the outflow rate is lower. If the term is introduced only in the outflow, the effect is not significant.

4.2. POLYTROPIC OUTFLOW COMING FROM THE REGION OF THE MAXIMUM PRESSURE

In this case, the inflow parameters are chosen from region **I** (see [21]) so that the shocks do not form. Here, the inflow passes through the inner sonic point only. The outflow is assumed to be originated from the regions where the polytropic inflow has a maximum pressure. This assumption is justified, since it is expected that winds would get the maximum kick at this region. Figure 6a shows a typical solution. The arrowed solid curve shows the inflow and the dotted arrowed curves show the outflows for $\gamma_o = 1.3$

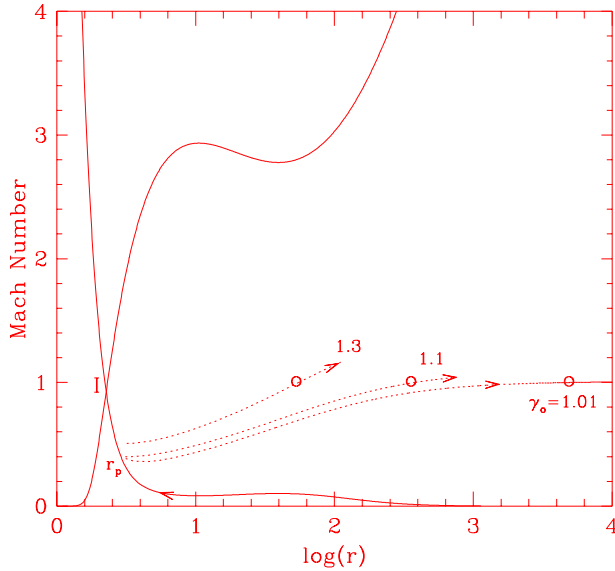


Fig. 6a: Few typical solutions for outflows forming out of an advective disk which does not include a standing shock wave. Incoming arrowed solid curve shows the inflow and the dashed arrowed curves with outgoing arrows show the outflows for $\gamma_o = 1.3$ (top), 1.1 (middle) and 1.01 (bottom). At r_p , thermal pressure of the inflow is maximum.

(top), 1.1 (middle) and 1.01 (bottom). The ratio $R_{\dot{m}}$ in these cases is given by 0.66, 0.30 and 0.09 respectively. The specific energy and angular momentum are chosen to be $\mathcal{E} = 0.00584$ and $\lambda = 1.8145$ respectively. The pressure maximum occurs outside the inner sonic point at r_p when the flow is still subsonic. Figure 6b shows the variation of thermal pressure of the flow with radial distance. The peak is clearly visible. Since the pressure maximum occurs very close to the black hole as compared to the location of the shock, the area of the outflow is smaller, but the radial velocity as well as the density of matter at the base of the outflow are much higher. As a result the outflow rate is exorbitantly higher compared to the shock case. Figure 7 shows the ratio $R_{\dot{m}}$ as a function of γ_o for various choices of the compression ratio R_{comp} of the outflowing gas at the pressure maximum: $R_{comp} = 2$ for the rightmost curve and 7 for the leftmost curve. We have purposely removed the solutions with $R_{\dot{m}} > 1$, because the solution should be inherently time-dependent (see, eq. 24b) in these cases and a steady state approach is not supposed to be trusted completely. This is different from the results of §4.1, where shocks are considered, since $R_{\dot{m}}$ is non-monotonic

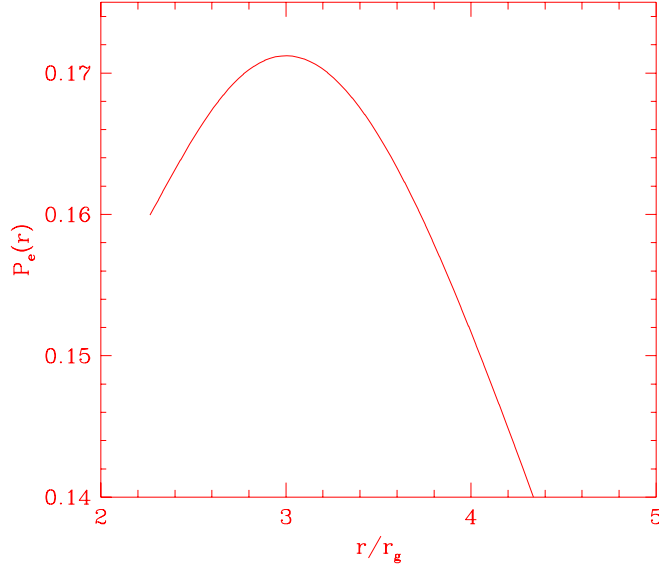


Fig. 6b: Variation of thermal pressure P_e of the incoming flow with radial distance. In a shock-free hydrodynamic flow, winds may form from the region around the pressure maximum.

in that case.

It is also found that in some range of parameters, the very high massflow could take place even for smaller compression ratios especially when the sonic point of the outflow r_o is right outside the pressure maximum. These cases can cause runaway instabilities by rapidly evacuating the disk. They may be responsible for quiescent states in X-ray novae systems (GS2000+25, GRS 1124-683) [27-28] and also in some systems with massive black holes (Sgr A*) [29-30]. Strong winds are suspected to be present in Sgr A* at our galactic center [29-30]. We show that when the inflow rate itself is low (as in the case for Sgr A*), the mass outflow rate is very high, almost to the point of evacuating the disk. Thus we think that any explanation of spectral properties of our galactic center (Sgr A*) should include winds using our model.

The location of maximum pressure being close to the black hole, it may be generally very difficult to generate the outflow from this region. Thus, it is expected that the ratio $R_{\dot{m}}$ would be larger when the maximum pressure is located farther out. This is exactly what we see in Fig. 8, where we plot $R_{\dot{m}}$ against the location of the pressure maximum (solid curve). Secondly, if our guess that the outflow rate could be related to the pressure is correct,

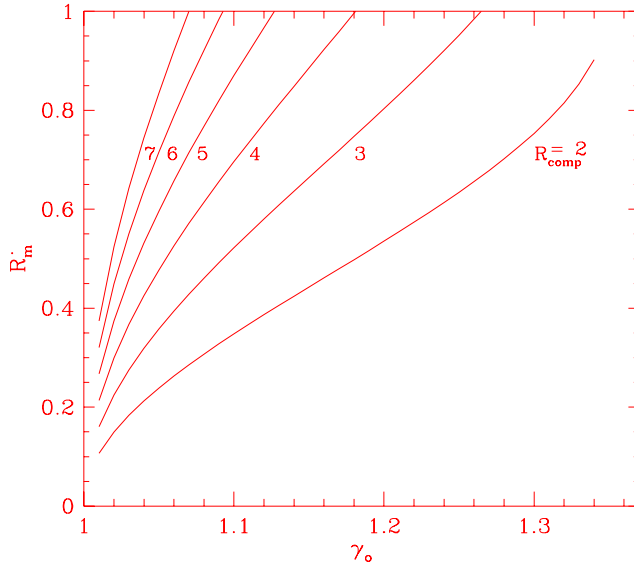


Fig. 7: $R_{\dot{m}}$ as a function of outflowing polytropic index γ_o for various choices of the compression ratio R_{comp} of the outflowing gas at the pressure maximum. From bottom to top curve, $R_{comp} = 2, 3, 4, 5, 6$ & 7 respectively. .

then the rate should increase as the pressure at the maximum rises. That is also observed in Fig. 8. We plot here $R_{\dot{m}}$ as a function of the actual pressure at the pressure maximum (dotted curve). The mass loss is found to be a strongly correlated with the thermal pressure. Here we have multiplied non-dimensional thermal pressure by 1.5×10^{24} in order to bring it in the same scale.

4.3. ISOTHERMAL OUTFLOW COMING FROM THE POST-SHOCK ACCRETION DISK

In this case, the outflow is assumed to be isothermal. The temperature of the outflow is obtained from the proton temperature of the advective region of the disk. The proton temperature is obtained using the Comptonization, bremsstrahlung, inverse bremsstrahlung and Coulomb processes ([26] and references therein). Figure 9 shows the effective proton temperature and the electron temperature of the post-shock advective region as a function of the accretion rate (in units of Eddington rate, in logarithmic scale) of the Keplerian component of the disk. The diagram is drawn for a black hole of mass $10M_{\odot}$. Similar results can be obtained for black hole of any mass.

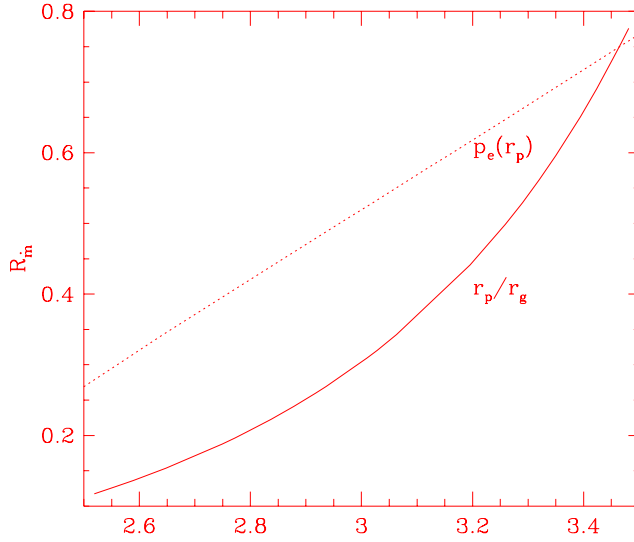


Fig. 8: Variation of R_{in} (solid) as a function of the location r_p of the maximum pressure and the non-dimensional pressure (dotted) $P_e(r_p)$ (multiplied by 1.5×10^{24} to bring to scale) are plotted.

The soft X-ray luminosity for stellar mass black holes or the UV luminosity of massive black holes is basically dictated by the Keplerian rate of the disk. It is clear that as the accretion rate of the Keplerian disk is increased, the advective region gets cooler as is expected.

In Fig. 10a, we show the ratio R_{in} as a function of the accretion rate (in units of Eddington rate) of the incoming flow for a range of the specific angular momentum. In the low luminosity objects the ratio is larger. Angular momentum is varied from $\lambda = 1.7$ (top curve), 1.725 (middle curve) and 1.75 (bottom curve). The specific energy is $\mathcal{E} = 0.003$. Here we have used the modified Rankine-Hugoniot relation as before (eq. 22). The ratio R_{in} is clearly very sensitive to the angular momentum since it changes the shock location rapidly and therefore changes the post-shock temperature very much. We also plot the outflux of angular momentum $F(\lambda) = \lambda \dot{m}_{in} R_{in}$ which has a maximum at intermediate accretion rates. In dimensional units, these quantities represent significant fractions of angular momentum of the entire disk and therefore the rotating outflow can help accretion processes. Curves are drawn for different λ as above. In Fig. 10b, we plot the variation of the ratio directly with the proton temperature of the advecting region. The outflow is clearly thermally driven. Hotter flow produces more winds

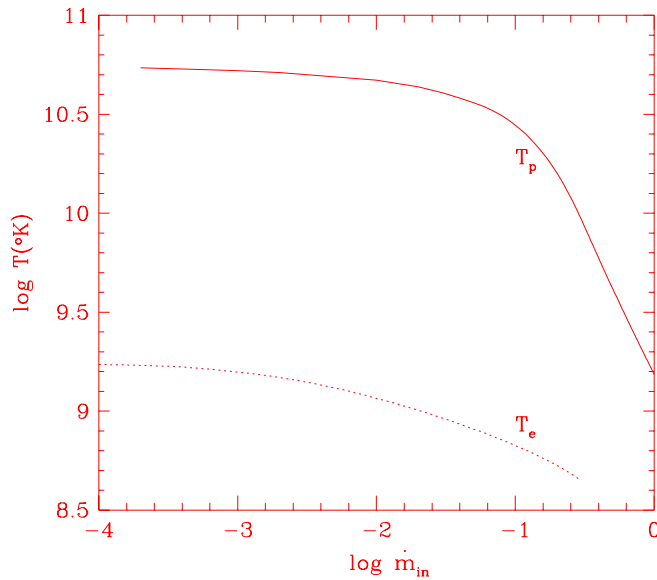


Fig. 9: Variation of effective proton (solid) and electron (dotted) temperatures in the advective regions of the accretion disk around a 10 solar mass black hole as functions of the accretion rates of the Keplerian flow. As Keplerian rate increases, both protons and electrons cool down.

as is expected. The angular momentum associated with each curve is same as before.

4.4. ISOTHERMAL OUTFLOW COMING FROM THE REGION OF THE MAXIMUM PRESSURE

This case produces very similar result as in the above case, except that like Section 4.2 the outflow rate becomes very close to a hundred percent of the inflow rate when the proton temperature is very high. Thus, when the accretion rate of the Keplerian flow is very small, the outflow rate becomes very high, close to evacuating the disk. As noted before, this may also be related to the quiescent state of the X-ray novae.

5. Conclusions

In this paper, we have computed the mass outflow rate from the advective accretion disks around galactic and extra-galactic black holes. Since the general physics of advective flows are similar around a neutron star, we believe that the conclusions may remain roughly similar provided the shock

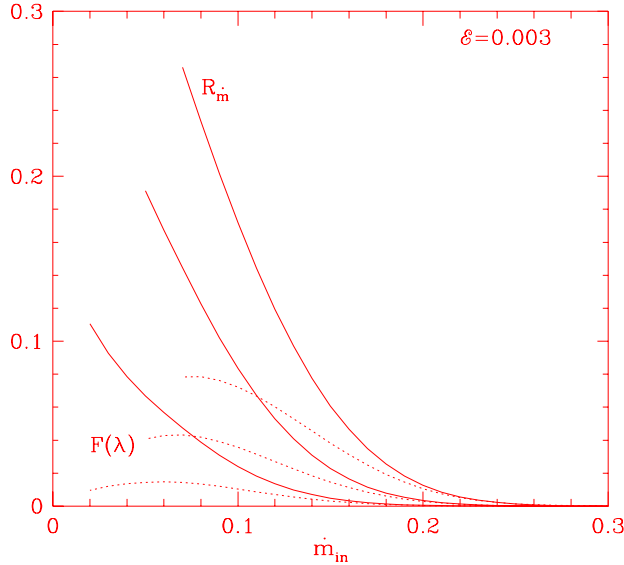


Fig. 10a: Variation of R_m as functions of the Eddington rate of the Keplerian component of the incoming flow for a range of the specific angular momentum. In the low luminosity objects the ratio is larger. The angular momentum flux $F(\lambda)$ of the outflow is also shown (dashed curve).

at X_{s3} forms, although the boundary layer (which corresponds to X_{s1} in [21] notation) of the neutron star, where half of the binding energy could be released, may be more luminous than that of a black hole and may thus affect the outflow rate. We have chosen a limited number of free parameters just sufficient to describe the inflow and only one extra parameter for the outflow. We find that the outflow rates can vary from a very few percentage of the inflow rate, to as much as the inflow rate (causing almost complete evacuation of the accretion disk) depending on the inflow parameters. For the first time, it became possible to use the exact transonic solutions for both the disks and the winds and combine them to form a self-consistent disk-outflow system. Although we present results when centrifugally supported boundary layers are considered around a black hole, it is evident that the result is general, namely, if such a barrier is produced by other means, such as pre-heating [31] or by pair-plasma pressure [32], outflows would also be produced [33-34]

The basic conclusions of this paper are the followings:

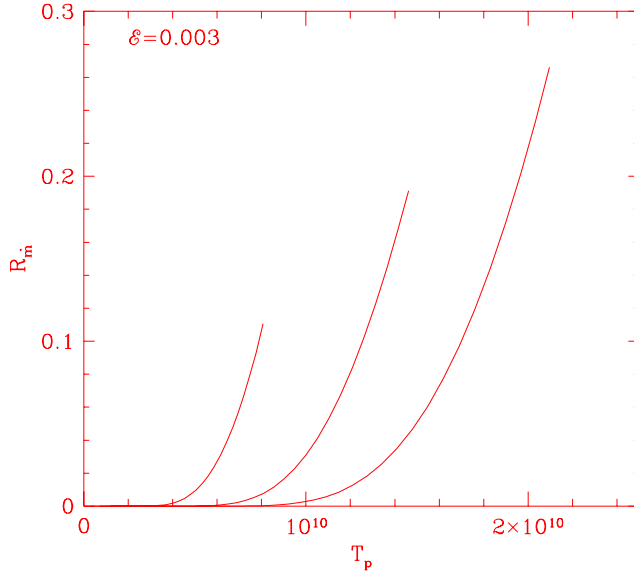


Fig. 10b: R_{in} as a function of the proton temperature T_p of the post-shock region. In (a), $\lambda = 1.7$ (top curve), $\lambda = 1.725$ (middle) and 1.75 (bottom curve).

- a) It is possible that most of the outflows are coming from the centrifugally supported boundary layer (CENBOL) of the accretion disks.
- b) The outflow rate generally increases with the proton temperature of CENBOL. In other words, winds are, at least partially, thermally driven. This is reflected more strongly when the outflow is isothermal.
- c) Even though specific angular momentum of the flow increases the size of the CENBOL, and one would have expected a higher mass flux in the wind, we find that the rate of the outflow is actually anti-correlated with the λ of the inflow. On the other hand, if the angular momentum of the outflow is reduced by hand, we find that the rate of the outflow is correlated with λ of the outflow. This suggests that the outflow is partially centrifugally driven as well.
- d) The ratio R_{in} is generally anti-correlated with the inflow accretion rate. That is, disks of lower luminosity would produce higher R_{in} .
- e) Generally speaking, supersonic region of the inflow do not have pressure maxima. Thus, outflows emerge from the subsonic region of the inflow, whether the shock actually forms or not.

In this paper, we assumed that the magnetic field is absent. Magnetized winds from the accretion disks have so far been considered in the context of

a Keplerian disk and *not* in the context of sub-Keplerian flows on which we concentrate here. Secondly, whereas the entire Keplerian disk was assumed to participate in wind formation, here we suggest that CENBOL is the major source of outflowing matter. It is not unreasonable to assume that CENBOL would still form when magnetic fields are present [1] and since the Alfvén speed is, by definition, higher compared to the sound speed, the acceleration, and therefore the mass outflow would also be higher than what we computed here. Such works would be carried out in future.

In the literature, not many results are present which deal with exact computations of the mass outflow rate. Molteni, Lanzafame & Chakrabarti [10], in their SPH simulations, found that the ratio could be as high as 15 – 20 per cent when the flow is steady. In Ryu, Chakrabarti & Molteni [12], 10 – 15 per cent of the steady outflow is seen and occasionally, even 150 of the inflow is found to be ejected in non-stationary cases. Our result shows that high outflow rate is also possible, especially for absence of shocks and low luminosities. In Eggum, Coroniti & Katz [9], radiation dominated flows showed $R_{\dot{m}} \sim 0.004$, which also agrees with our results when we consider high accretion rates (see, e.g., Fig. 9a). Observationally, it is very difficult to obtain the outflow rate from a real system, as it depends on too many uncertainties, such as filling factors and projection effects. In any case, with a general knowledge of the outflow rate, we can now proceed to estimate several important quantities. For example, it had been argued that the composition of the disk changes due to nucleosynthesis in accretion disks around black holes and this modified isotopes are deposited in the surroundings by outflows from the disks ([35-36] and references therein). Similarly, it is argued that outflows deposit magnetic flux tubes from accretion disks into the surroundings [37]. Thus a knowledge of outflows are essential in understanding varied physical phenomena in galactic environments.

Would our solution be affected if radiation pressure is included? A preliminary investigation with a Γ/r^2 force term (whose effect is to weaken gravity) suggests that for non-zero Γ in the inflow, the mass-loss rate changes significantly. This is because the shock location increases when Γ is increased. This in turn reduces the mass loss rate. On the other hand, the when Γ is non-zero in the outflow, the effect is not very high, since the outflow rate is generally driven by thermal effect of the *disk* and not the wind. Similarly, we see a significant reduction of the outflow when the average specific angular momentum of the outflow is reduced. This is expected since the outflow is partially centrifugally driven. This effect is stronger when the outflow is isothermal.

An interesting situation arises when the polytropic index of the outflow is large and the compression ratio of the flow is also very high. In this case, the flow virtually bounces back as the winds and the outflow rate can be

equal to the inflow rate or even higher, thereby evacuating the disk. In this range of parameters, most, if not all, of our assumptions may breakdown completely because the situation could become inherently time-dependent. It is possible that some of the black hole systems, including that in our own galactic centre, may have undergone such evacuation phase in the past and gone into quiescent phase.

So far, we made the computations around a Schwarzschild black hole. In the case of a Kerr black hole [15], the shock locations will come closer and the outflow rates should become higher. Similarly magnetic field will change the sonic point locations significantly [1]. The mass outflow rates in these conditions are being studied and the results would be reported elsewhere [38].

References

1. Chakrabarti, S. K. 1996, in *Accretion Processes on Black Holes*, Physics Reports, v. 266, No. 5 & 6, p 229
2. Chakrabarti, S. K. 1998, *Ind. J. Phys.* 72B(3), 183
3. Mirabel, I.F. & Rodríguez, L. F. 1994, *Nature* 371, 46
4. Ferrari, A. Trussoni, E., Rosner, R. & Tsinganos, K. 1985, *ApJ*, 294, 397
5. Fukue, J. 1982, *PASJ*, 34, 163
6. Contopoulos, J. 1995, *Ap.J.*, 446, 67
7. Königl, A. 1989, *Ap.J.*, 342, 208
8. Chakrabarti, S. K. & Bhaskaran, P. 1992, *MNRAS*, 255, 255
9. Eggum, G.E., Coroniti, F.V., Katz, J.I. 1985, *Ap.J.*, 298, L41
10. Molteni, D., Lanzafame, G. & Chakrabarti, S.K. 1994 *Ap.J.*, 425, 161
11. Molteni, D., Ryu, D. & Chakrabarti 1996, *Ap.J.*, 470, 460
12. Ryu, D., Chakrabarti, S.K., & Molteni, D. 1997, *Ap.J.*, 474, 378
13. Castor, J. I., Abott, D. C. & Klein, R. I. 1975, *Ap.J.*, 195, 157
14. Shapiro, S. & Teukolski, S. 1983, *Black Holes, White Dwarfs, and Neutron Stars: The Physics of Compact Objects* (John Wiley & Sons)
15. Chakrabarti, S. K. 1996, *MNRAS*, 471, 237
16. Chakrabarti, S. K., Titarchuk, L. G., Kazanas, D., & Ebisawa, K., 1996, *Astron. & Astrophys. Suppl. Series*, 120, 163
17. Crary, D. J. et. all. 1996, *Ap.J.*, L71
18. Molteni, D., Sponholtz, H., Chakrabarti, S. K., 1996, *Ap.J.*, 457,805
19. Strohmayer, T. E., Zhang, J. H. Swank, Smale, A. 1996, *Ap.J.*, 469, L9
20. Lanzafame, G., Molteni, D., Chakrabarti, S. K., 1998, *MNRAS*, 299,799
21. Chakrabarti, S. K. 1989, *Ap.J.*, 347, 365
22. Chakrabarti, S. K. 1998, in *Observational Evidence for Black Holes in the Universe*, Ed. S.K. Chakrabarti (Kluwer Academic: Holland) , p. 19
23. Das, T.K., 1998, in *Observational Evidence for Black Holes in the U niverse*, Ed. S.K. Chakrabarti (Kluwer Academic: Holland), p. 113
24. Paczyński, B. & Wiita, P. J. 1980, *A & A*, 88, 23
25. Tarafdar, S.P. 1988, *Ap.J.*, 331, 932
26. Chakrabarti, S. K. 1997, *Ap.J.*, 484, 313
27. Tanaka, Y., 1995, *Nature*, 375,659
28. Ueda, Y., Ebisawam K. & Done, C. 1994, *PASJ*, 46, 107

29. Genzel, R. et. al. (1994) *Rep. Prog. Phys.* **57,417**
30. Eckart, A. & Genzel, R. 1997, MNRAS, 284,576
31. Chang, K.M. & Ostriker, J.P. 1985, Ap.J., 288, 428
32. Kazanas, D. & Ellison, D. C. 1986, Ap.J., 304, 178
33. Das, T. K. 1999 MNRAS (**308,201**)
34. Das, T. K. 1999 MNRAS (submitted).
35. Chakrabarti, S.K. and Mukhopadhyay, B. 1998, A&A, 344,105
36. Hogan C.J., Applegate J.H., 1987, Nature, 390, 236
37. Daly, R.A. & Loeb, A. 1990, Ap.J., 364, 451
38. Das, T.K., 1999, in preparation.